ChemComm

Check for updates

A high-contrast polymorphic difluoroboron luminogen with efficient RTP and TADF emissions†

Xin Wang, [ID] [ab] Xiaofu Wu, [ID] [a] Tong Wang, [ab] Yuliang Wu, [ab] Haiyang Shu, [ab] Zhiqiang Cheng, [ab] Lei Zhao, [a] Hongkun Tian, [ab] Hui Tong [ID] *[ab] and Lixiang Wang [ID] *[ab]

A simple *N,S*-chelated four-coordinated difluoroboron-based emitter is reported with three polymorphs, which emit high contrast green (G), yellow (Y) and red (R) light. Interestingly, the G and R-Crystals show different thermally activated delayed fluorescence (TADF) at 530 nm and 630 nm with a remarkable emission spectral shift of up to 100 nm, while the Y-Crystal exhibits room temperature phosphorescence (RTP) at around 570 nm with a high solid-state quantum yield of 77%. Single crystal analysis and theoretical calculations reveal that different molecular conformations and packing modes lead to distinct triplet exciton conversion channels.

Organic luminescent materials with both thermally activated delayed fluorescence (TADF) and metal-free room temperature phosphorescence (RTP) in the solid state are highly attractive inspired by their widespread applications in the fields of organic light emitting diodes, organic solid-state lasers, sensors, bio-imaging and anti-counterfeiting.[1–4] In TADF emitters, the triplet excitons can be converted into spin-allowed singlet excitons for delayed fluorescence, through reverse intersystem crossing (RISC). Similar to TADF, organic RTP can also utilize triplet excitons for light emission, which, however, results from the direct radiative decay of triplet excited states.[5,6] Until now, regulation of the emission behavior of organic luminescent materials is still mainly based on molecular structural modification, which can tune their lifetime, efficiency, and color, and even realize the modulation of TADF and RTP.[7,8] On the other hand, photophysical properties of a given molecular system in the solid state can also be significantly influenced by both molecular conformation and packing.[9,10] Notably, the luminescence color can be dramatically affected by different conformations and

packing modes in multiple crystalline polymorphs. In most cases, these polymorphs generally exhibit fluorescence,[11] TADF[12,13] or RTP emission.[14,15] Whereas, modulation of the triplet excitons to display controllable RTP or TADF through different conformations and packing modes is quite rare.[16–19] Phenothiazine with quasi-axial (ax) and quasi-equatorial (eq) conformations has been used as the donor unit to construct several donor–acceptor (D–A) type molecules with different TADF or RTP emissions in the crystal, amorphous and doped film states.[20–22] Recently, Takeda and coworkers reported a phenoselenazine-based D–A type emitter to form three polymorphs with different emission colors; however, their photoluminescence quantum yields (PLQYs) are rather low (less than 3%), and no in-depth photophysical studies were performed for these polymorphs.[23] Fu and coworkers successfully obtained two polymorphs of βCBF2 with both TADF and RTP emission and PLQYs of up to 26% in the solid state.[16] Chi *et al.* also realized a series of TADF and RTP organic polymorphs with PLQYs up to 28% based on a D–A type molecule.[17] However, luminescent polymorphs exhibiting TADF and RTP emission with both high contrast multi-color emission and high photoluminescence yield are still an elusive challenge.

In this paper, we developed a D–A type molecule DMAC-PSBF2 with three polymorphs by using 9,10-dihydro-9,9-dimethylacridine (DMAC) as a donor (D) and *N,S*-thioamide difluoroboron[24] as an acceptor (A). Similar as phenothiazine, DMAC derivatives with folded or planar conformations have been reported,[25,26] which may facilitate the formation of polymorphs with different conformations. Unlike popular *N,O*- and *O,O*-chelated four-coordinated difluoroboron-based emitters,[27,28] the introduction of a S atom will provide a heavy atom effect and contribute to the formation of triplet excitons and phosphorescence. Three polymorphs with high contrast emission colors exhibiting green (G-Crystal, 530 nm), yellow (Y-Crystal, 570 nm) and red (R-Crystal, 630 nm) emission are successfully obtained with the PLQYs of up to 77%. Moreover, stimulated by the different molecular conformations and packing modes, the lowest singlet and triplet states and their energy gaps have been

ª State Key Laboratory of Polymer Physics and Chemistry, Changchun Institute of Applied Chemistry, Chinese Academy of Sciences, Changchun 130022, P. R. China. E-mail: chemtonghui@ciac.ac.cn, lixiang@ciac.ac.cn

ᵇ University of Science and Technology of China, Hefei 230026, P. R. China

significantly influenced, leading to different photophysical mechanisms with TADF character of the G and R-Crystals, and RTP character of the Y-Crystal.

The photophysical properties of DMAC-PSBF2 in dilute n-hexane solution (1×10^{-6} M) are shown in Fig. 2a. The UV-visible absorption spectrum has three absorption peaks at 290 nm, 366 nm and 435 nm. The high-energy absorption bands at 290 nm and 366 nm can be assigned to the $\pi \rightarrow \pi^*$ transition of the donor and acceptor units, respectively, while the low-energy absorption band around 435 nm is identified as the intermolecular charge transfer (ICT) transitions between the D and A units. The steady-state PL spectrum under an argon atmosphere shows a structure-less band at room temperature with the maximum emission located at 542 nm with a quantum yield of 89%, which can be assigned as ICT transition (Fig. 2a). The PL intensity significantly weakens upon exposure to oxygen compared to that under an argon atmosphere (Fig. S1a, ESI†). Meanwhile, the transient PL decay curve of the solution exhibits double-exponential decay with a delayed lifetime of 1.41 μs under degassed conditions, but the delayed component decreased significantly under oxygen conditions (Fig. S1b, ESI†), suggesting that the triplet excitons participate in the luminescence. The delayed component in the transient PL decay curve at 300 K increased compared to those at 77 K (Fig. S1c, ESI†), indicating TADF mechanism. Based on the onset wavelengths of the fluorescence (300 K) and phosphorescence spectra (77 K) (Fig. S1d, ESI†), the S_1 and T_1 level of the solution state can be calculated to be 2.55 and 2.53 eV, so ΔE_{ST} = 0.02 eV. The small ΔE_{ST} may facilitate the efficient reverse intersystem crossing (RISC) process and promote TADF emission.[29] The film of DMAC-PSBF2 doped in rigid matrices (PMMA) exhibits the maximum peak at 560 nm (Fig. 2a), which also exhibits a high PLQY up to 28% with the long lifetime of 1.91 μs at room temperature. The PL intensity of the doped film decreased significantly with the increase of temperature. Simultaneously, the delayed component of the transient PL decay spectra decreases as the temperature rises (Fig. S2a and b, ESI†). Considering that the non-radiative deactivation process was promoted at higher temperature and may seriously quench RTP emission, the emission of the doped film can be ascribed to RTP.[13] Furthermore, its steady-state and delayed PL spectra (100 μs delay) at 300 K and 50 K were overlapped, suggesting that the emission bands were derived from the same excited state (Fig. S6a, ESI†), confirming RTP emission.[30] We found the prompt fluorescence band of the doped film through time-resolved photoluminescence spectra, which emerge at 537 nm. Meanwhile, at longer delay times, a red-shifted peak appeared at 567 nm, assigned to phosphorescence (Fig. S2c and d, ESI†). The S_1 and T_1 levels were calculated to be 2.59 eV and 2.40 eV and the ΔE_{ST} of the doped film is 0.19 eV. The much larger ΔE_{ST} value compared to that of its solution is beneficial for its RTP property (Table 1).

A single crystal of DMAC-PSBF2 was cultivated to investigate its emission behavior in its crystal state. To our surprise, three distinct single crystals with green, yellow and red emission under ultraviolet lamp (namely G-Crystal, Y-Crystal and R-Crystal, respectively) were obtained by slowly evaporating

Table 1 Photophysical parameters of DMAC-PSBF2 in different states

State	λ_F (nm)	λ_P (nm)	τ_{DF} (μs)	τ_{Phos} (μs)	Φ^e (%)	E_S/E_T^f (eV)	ΔE_{ST}^g (eV)
Solution^a	542	546^d	0.51	—	89	2.55/2.53	0.02
Doped film^b	537^c	567^c	—	1.91	28	2.59/2.40	0.19
Crystal G	530^c	541^c	3.10	—	58	2.53/2.46	0.07
Crystal Y	—	570^c	—	0.47	77	—/2.38	—
Crystal R	630^c	633^c	0.72	—	23	2.16/2.14	0.02

^{a} Measured in n-hexane solution (1×10^{-5} M). ^{b} 1 wt% doped in PMMA. ^{c} The fluorescence and phosphorescence emission peaks are confirmed by the time-resolved PL spectra at 50 K. ^{d} phosphorescence spectra measured at 77 K under Ar conditions. ^{e} Measured at room temperature under Ar. ^{f} Singlet (E_S) and triplet (E_T) energies estimated from fluorescence and phosphorescence onset wavelengths, respectively. ^{g} $\Delta E_{ST} = E_S - E_T$.

mixed solutions of dichloromethane/n-hexane, dichloromethane/methanol and toluene/n-hexane, respectively (Fig. 1). The corresponding PL emission peaks of the G-, Y- and R-Crystals are located at 530, 570 and 630 nm (Fig. 2b). The emission colors have sharp contrasts of the three polymorphs, with the emission peaks of the R-Crystal red-shifted by 60 nm and 100 nm compared to that of the Y- and G-Crystals. The PLQYs of the G-, Y- and R-Crystals are determined to be 58%, 77% and 23%, respectively, these solid-state quantum yields are much larger compared to those of most polymorphic materials.[11–23] Notably, the transient PL decay curves of the three polymorphs show second-order exponential decay and the long lifetimes of the G, Y and R-Crystals are identified as 3.10 μs, 0.47 μs and 0.72 μs under Ar, but the lifetimes were all decreased when they were exposed to oxygen (Fig. S4, ESI†), which indicates that the triplet excitons participate in the emission. We further measured temperature-dependent transient and steady-state PL spectra, along with time-resolved PL spectra
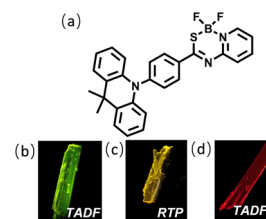

Fig. 1 (a) Molecular structure of the target compound DMAC-PSBF2. (b–d) Photographs of the green, yellow and red microcrystals under UV excitation.
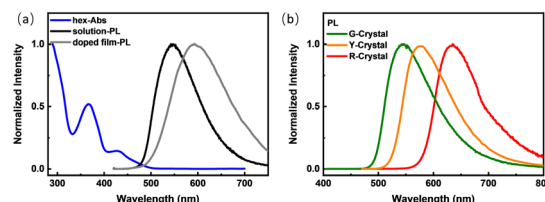

Fig. 2 (a) The absorption (blue line) and steady-state PL spectra of DMAC-PSBF2 in n-hexane solution (dark line) (1×10^{-6} M) and PL spectrum of the film (gray line) doped in PMMA (1 wt%). (b) The steady-state PL spectra of green (green line), yellow (yellow line) and red micro-crystals (red line), respectively.

(300 K and 50 K) to investigate the properties of the triplet excited states of the three polymorphs. The PL intensity and delayed component of the Y-Crystal decrease significantly with increased temperature (Fig. S3c and d, ESI†), indicating its RTP emission as its doped film. Furthermore, its steady-state and delayed PL spectra (100 μs delay) at 300 K and 50 K are all overlapped, suggesting that the emission bands are derived from the same excited state (Fig. S6b, ESI†), confirming the RTP property.[30] In sharp contrast, the delayed component of the transient PL decay spectra of G-Crystal and R-Crystal increase as the temperature rises (Fig. S3a and e, ESI†). The PL intensity of G-Crystal is enhanced obviously with the increased temperature (Fig. S3b, ESI†), indicating the TADF character.[22] R-Crystal presents an opposite trend for the PL intensity (Fig. S3f, ESI†), implying that at low temperatures, phosphorescence is the dominant process, and similar phenomena have been reported for several TADF materials.[31,32] At 300 K, both the prompt and delayed emission bands of the G- and R-Crystals are almost identical to the steady-state PL spectra (Fig. S5a and e, ESI†), implying the TADF mechanism too, in which RISC can be activated at room temperature.[20] According to the onset wavelengths of the prompt fluorescence and phosphorescence spectra (Fig. S5, ESI†), the ΔE_{ST} values are calculated to be 0.07 eV and 0.02 eV for G-Crystal and R-Crystal, respectively. The small ΔE_{ST} values are of benefit for RISC and TADF process.[23] These results indicate that the emission mechanisms are different for the three polymorphs, the G- and R-Crystals exhibit TADF, while the Y-Crystal displays RTP.

Single crystal X-ray diffraction (XRD) measurements of the three polymorphs were all carried out. G-, Y- and R-Crystals all have large dihedral angles of over 80° between the donor DMAC and the acceptor PSBF2 segments (89°, 80° and 86° for G-, Y- and R-Crystals, respectively). The DMAC fragment conformations in the three crystals are different, the G- and Y-crystals exhibit crooked forms with the twist angles of 39° and 43°, while the R-Crystal possesses a much smaller one of just 10° (Fig. 3). The different conformations will play evident roles to affect their conjugation degrees and hence their energy levels.[25,26] DMAC-PSBF2 molecules are packed in different arrangements of different polymorphs. G-Crystal belongs to the triclinic space group $P\bar{1}$, the π–π stacking distance of the adjacent dimers is 3.73 Å (Fig. 3d). Multiple intermolecular
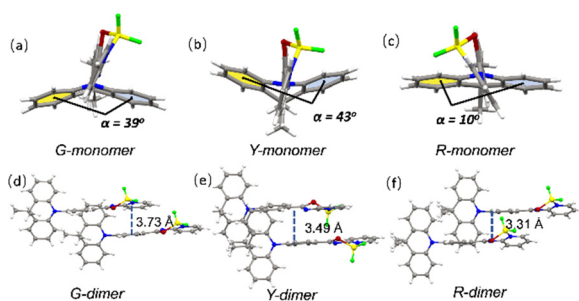

Fig. 3 The monomer molecular structures in single crystals of G-crystal (a), Y-crystal (b) and R-crystal (c). The adjacent dimers in single crystals of G-crystal (d), Y-crystal (e) and R-crystal (f).

interactions can be observed within the molecular cell, including C–H⋯π (2.69 Å), C–H⋯F (2.65 Å) and C–H⋯S (3.00 Å) interactions (Fig. S7, ESI†). R-Crystal is an orthorhombic crystal with the *Pbca* space group, which shows a shorter π–π stacking distance of 3.31 Å between the neighboring molecules (Fig. 3f). There exist less molecular interactions between the paired dimers of C–H⋯F (2.42 Å) and C–H⋯π (2.88 Å). The close distance between the adjacent molecules, combined with the large bathochromic band compared to those of the other two polymorphs, suggests the formation of an excimer.[33,34] Y-Crystal belongs to the monoclinic space group $P21/c$, the π–π stacking distance between the two adjacent molecules is 3.49 Å (Fig. 3e). It has substantial C–H⋯F (2.40 Å, 2.41 Å, and 2.53 Å), C–H⋯π (2.68 Å, 2.79 Å, and 2.88 Å) and S⋯π (3.46 Å) interactions, forming a three-dimensional framework (Fig. S7, ESI†). Accordingly, it has the largest density of 1.439 g cm^{-3} compared to that of the G-Crystal (1.379 g cm^{-3}) and R-Crystal (1.365 g cm^{-3}). Compared to the G- and R-Crystals, short dense intermolecular contacts in the Y-Crystal provide a favorable rigid environment to suppress the vibrational approaches and construct perfect crystallization to exclude the erosion from external moisture and oxygen, promoting the RTP character.[35,36]

To gain deep insight into the effect of molecular packing on their different PL behaviors in the three polymorphs, density functional theory (DFT) and time-dependent DFT (TD-DFT) calculations were carried out based on monomer and dimer structures derived from the three crystals. All the T_1 levels of three monomers in different crystals are almost the same and around 3.00 eV, while the S_1 levels are quite different (Fig. S12, ESI†), which is consistent with the natural transition orbital (NTO) analysis of their S_0–S_1 and S_0–T_1 transition. The S_1 states of the monomers exhibit a predominantly CT character with holes and particles locating on the DMAC and PSBF2 fragments, respectively, which should be influenced by their conformations significantly due to the different DMAC conformations and donor–acceptor twisted structures.[25,26] However, their T_1 states have clear LE character and are mainly located on the acceptor unit, leading to the similar T_1 energy levels (Fig. S10, ESI†). For the monomer in the Y-Crystal, its S_1 of 3.25 eV is the highest among the three monomers, resulting in the largest ΔE_{ST} value of 0.25 eV, which may obstruct the RISC process. Besides, a large SOC value (6.23 cm^{-1}) of the Y-Crystal between its T_1 and S_0 will support an effective radiative transition of T_1 excitons, leading to efficient RTP emission from its T_1 state,[37,38] while for the monomers in the G- and R-Crystals, smaller ΔE_{ST} values (0.17 and 0.08 eV) are obtained due to their lower S_1 energy levels, supporting their efficient RISC process and TADF emission behaviors (Fig. S12, ESI†). However, the TADF emission of the R-Crystal around 630 nm is even much red-shifted compared to the RTP emission of the Y-Crystal (around 570 nm), which is rather strange considering its higher S_1 energy level (3.08 eV) than the T_1 (3.00 eV) of the Y-Crystal. Further inspection of the dimer of the R-Crystal reveals that the particle distributions of its S_1 and T_1 states have apparent intermolecular characteristics, which leads to reduced S_1 (2.94 eV) and T_1 (2.90 eV) energy levels and an even smaller ΔE_{ST} of 0.04 eV,

implying the excimer emission nature for the significantly red-shifted emission of the R-Crystal (Fig. S11, ESI†).[33,34] On the other hand, for the dimers in the G- and Y-Crystals, the S_1 state of the G-Crystal has the same hole–particle distributions as its monomer (Fig. S10 and S11, ESI†), and this is also the case for the T_1 state of the Y-Crystal. Furthermore, the energy levels of the dimers of the G- and Y-Crystals are quite similar to those of their monomers (Fig. S12, ESI†), implying that the emission properties of the G- and Y-Crystals are dominated by the monomer behavior, which is also supported by the fact that the emission spectra and mechanism of G-Crystal and Y-Crystal are similar to those in solution and doped films, respectively.

In conclusion, we designed and synthesized a novel organic molecule DMAC-PSBF2 with three polymorphs. Three different single crystals called G-Crystal, Y-Crystal and R-Crystal provide high contrast emission peaks from 530–630nm, and their PLQYs are up to 77%. More importantly, the behavior of triplet excitons can be controlled by the aggregation states, which will affect their emission character of TADF or RTP. Single crystal data and theoretical studies demonstrate that the molecular conformations and packing modes determine their transition patterns. The synergistic effects of the conformations and packing modes endow the three polymorphs with different emission behaviors, the G and R-Crystals exhibit TADF, while the Y-Crystal shows RTP. These results highlight the significant role of molecular conformations and packing modes in regulating the behavior of excited-states, and also provide a new molecular design and tuning approach for obtaining efficient switchable solid-state TADF and RTP materials.

Conflicts of interest

There are no conflicts to declare.

Notes and references

1 G. Hong, X. Gan, C. Leonhardt, Z. Zhang, J. Seibert, J. Busch and S. Bräse, *Adv. Mater.*, 2021, **33**, 2005630.
2 C. Yan, X. Wang and L. Liao, *Adv. Sci.*, 2022, **9**, 2200525.
3 F. Li, M. Wang, S. Liu and Q. Zhao, *Chem. Sci.*, 2022, **13**, 2184.
4 Y. Wang, H. Gao, J. Yang, M. Fang, D. Ding, B. Tang and Z. Li, *Adv. Mater.*, 2021, **33**, 2007811.
5 F. Fang, L. Zhu, M. Li, Y. Song, M. Sun, D. Zhao and J. Zhang, *Adv. Sci.*, 2021, **8**, 2102970.
6 W. Zhao, Z. He and B. Tang, *Nat. Rev. Mater.*, 2020, **5**, 869.
7 K. Ling, H. Shi, H. Wang, L. Fu, A. Lv, K. Huang, W. Ye, M. Gu, C. Ma, X. Yao, W. Jia, J. Zhi, W. Yao, Z. An, H. Ma and W. Huang, *Adv. Opt. Mater.*, 2019, **7**, 1901076.
8 C. Chen, R. Huang, A. Batsanov, P. Pander, Y. Hsu, Z. Chi, F. Dias and M. Bryce, *Angew. Chem., Int. Ed.*, 2018, **57**, 16407.
9 Q. Li and Z. Li, *Acc. Chem. Res.*, 2020, **53**, 962.
10 L. Tu, Y. Xie and Z. Li, *J. Phys. Chem. Lett.*, 2022, **13**, 5605.
11 C. Zhu, Q. Luo, Y. Shen, C. Lv, S. Zhao, X. Lv, F. Cao, K. Wang, Q. Song, C. Zhang and Y. Zhang, *Angew. Chem., Int. Ed.*, 2021, **60**, 8510.
12 K. Zheng, F. Ni, Z. Chen, C. Zhong and C. Yang, *Angew. Chem., Int. Ed.*, 2020, **59**, 9972.
13 W. Yang, Y. Yang, L. Zhan, K. Zheng, Z. Chen, X. Zeng, S. Gong and C. Yang, *Chem. Eng. J.*, 2020, **390**, 124626.
14 L. Gu, H. Shi, L. Bian, M. Gu, K. Ling, X. Wang, H. Ma, S. Cai, W. Ning, L. Fu, H. Wang, S. Wang, Y. Gao, W. Yao, F. Huo, Y. Tao, Z. An, X. Liu and W. Huang, *Nat. Photonics*, 2019, **13**, 406.
15 H. Liu, W. Liu, N. Ando, S. Yamaguchi and H. Zhang, *J. Mater. Chem. C*, 2021, **9**, 2738.
16 S. Li, L. Fu, X. Xiao, H. Geng, Q. Liao, Y. Liao and H. Fu, *Angew. Chem., Int. Ed.*, 2021, **60**, 18059.
17 W. Li, Q. Huang, Z. Mao, J. Zhao, H. Wu, J. Chen, Z. Yang, Y. Li, Z. Yang, Y. Zhang, M. Aldred and Z. Chi, *Angew. Chem., Int. Ed.*, 2020, **59**, 3739.
18 X. Wang, W. Guo, H. Xiao, Q. Yang, B. Chen, Y. Chen, C. Tung and L. Wu, *Adv. Funct. Mater.*, 2020, **30**, 1907282.
19 L. Zhan, Z. Chen, S. Gong, Y. Xiang, F. Ni, X. Zeng, G. Xie and C. Yang, *Angew. Chem., Int. Ed.*, 2019, **58**, 17651.
20 M. Okazaki, Y. Takeda, P. Data, P. Pander, H. Higginbotham, A. Monkmanb and S. Minakata, *Chem. Sci.*, 2017, **8**, 2677.
21 Y. Takeda, T. Kaihara, M. Okazaki, H. Higginbotham, P. Data, N. Tohnai and S. Minakata, *Chem. Commun.*, 2018, **54**, 6847.
22 P. Data, M. Okazaki, S. Minakata and Y. Takeda, *J. Mater. Chem. C*, 2019, **7**, 6616.
23 S. Goto, Y. Nitta, N. Decarli, L. Sousa, P. Stachelek, N. Tohnai, S. Minakata, P. Silva, P. Data and Y. Takeda, *J. Mater. Chem. C*, 2021, **9**, 13942.
24 B. Jędrzejewska, A. Zakrzewska, G. Mloston, S. Budzak, K. Mroczynska, A. M. Grabarz, M. A. Kaczorowska, D. Jacquemin and B. Osmiałowski, *J. Phys. Chem. A*, 2016, **120**, 4116.
25 K. Wang, C. Zheng, W. Liu, K. Liang, Y. Shi, S. Tao, C. Lee, X. Ou and X. Zhang, *Adv. Mater.*, 2017, **29**, 1701476.
26 S. Li, Y. Xie, A. Li, X. Li, W. Che, J. Wang, H. Shi and Z. Li, *Sci. China: Mater.*, 2021, **64**, 2813.
27 X. Wang, H. Li, X. Wu, H. Shu, H. Tian, H. Tong and L. Wang, *J. Mater. Chem. C*, 2021, **9**, 14133.
28 D.-H. Kim, A. D'Aléo, X.-K. Chen, A. D. S. Sandanayaka, D. Yao, L. Zhao, T. Komino, E. Zaborova, G. Canard, Y. Tsuchiya, E. Choi, J. W. Wu, F. Fages, J.-L. Brédas, J.-C. Ribierre and C. Adachi, *Nat. Photonics*, 2018, **12**, 98.
29 H. Lee, K. Lee and J. Lee, *Adv. Opt. Mater.*, 2020, **8**, 2001025.
30 Z. Lin, R. Kabe, K. Wang and C. Adachi, *Nat. Commun.*, 2020, **11**, 191.
31 (a)L. Yu, Z. Wu, C. Zhong, G. Xie, Z. Zhu, D. Ma and C. Yang, *Adv. Opt. Mater.*, 2017, **5**, 1700588.
32 X. Wei, Y. Chen, R. Duan, J. Liu, R. Wang, Y. Liu, Z. Li, Y. Yi, Y. Yamada-Takamura, P. Wang and Y. Wang, *J. Mater. Chem. C*, 2017, **5**, 12077.
33 J. Wang, L. Peng, Z. Liu, X. Zhu, L. Niu, G. Cui and Q. Yang, *J. Phys. Chem. Lett.*, 2022, **13**, 1985.
34 Y. Gong, P. Zhang, Y. Gu, J. Wang, M. Han, C. Chen, X. Zhan, Z. Xie, B. Zou, Q. Peng, Z. Chi and Z. Li, *Adv. Opt. Mater.*, 2018, **6**, 1800198.
35 Y. Xie, Y. Ge, Q. Peng, C. Li, Q. Li and Z. Li, *Adv. Mater.*, 2017, **29**, 1606829.
36 Y. Gong, G. Chen, Q. Peng, W. Yuan, Y. Xie, S. Li, Y. Zhang and B. Tang, *Adv. Mater.*, 2015, **27**, 6195.
37 Y. Tao, R. Chen, H. Li, J. Yuan, Y. Wan, H. Jiang, C. Chen, Y. Si, C. Zheng, B. Yang, G. Xing and W. Huang, *Adv. Mater.*, 2018, **30**, 1803856.
38 Z. Yu, Y. Wu, L. Xiao, J. Chen, Q. Liao, J. Yao and H. Fu, *J. Am. Chem. Soc.*, 2017, **139**, 6376.